

Systematic study of laser-assisted proton radioactivity from deformed nuclei

Jun-Hao Cheng,¹ Yi Li,² and Tong-Pu Yu^{1,*}

¹*Department of Physics, National University of Defense Technology, 410073 Changsha, People's Republic of China*

²*Nuclear Power Institute of China, 610041 Chengdu, People's Republic of China*



(Received 4 September 2021; revised 23 December 2021; accepted 27 January 2022; published 16 February 2022)

In the present work, we systematically study the effect of ultra-intense laser fields on proton radioactivity of deformed proton emitters with the state-of-the-art Gaussian laser and the latest evaluated nuclear properties table. The calculated results indicate that ultra-intense laser fields affect the proton radioactivity half-life by changing the proton radioactivity penetration probability to some small but finite extent, and the ^{108}I is the most sensitive parent nuclei to the strong laser pulse. Moreover, we found that the released energy of proton radioactivity is negatively related to the rate of change of the proton radioactivity penetration probability. Finally, we investigate the effect of the asymmetric chirp-laser pulse on the average rate of change in proton radioactivity penetration probability. It is shown that the rational use of positive chirp is equivalent to increasing the laser intensity by two orders of magnitude.

DOI: [10.1103/PhysRevC.105.024312](https://doi.org/10.1103/PhysRevC.105.024312)

I. INTRODUCTION

Laser, the electromagnetic wave emitted by electrons in atoms that absorb energy and transits from the high-energy state to the low-energy state, was first invented by Maiman in 1960. Since it was manufactured, laser technology has shown its irreplaceable role in many fields such as medicine, nuclear physics, electron-positron pair production, fusion ignition, and inertial confinement fusion [1–6]. Nowadays, the advent of chirped pulse amplification techniques [7], which was awarded the Nobel Prize in Physics in 2018, makes laser fields being with a wide range of frequencies high intensities and durations [8]. Excitingly, in July 2019, a laser pulse with a peak intensity of more than $5.5 \times 10^{22} \text{ W/cm}^2$ was produced [9], and the peak intensity of the laser pulse was increased to 10^{23} W/cm^2 in May 2021 [10]. Moreover, the extreme light infrastructure for nuclear physics (ELI-NP), one of the primary scientific goals of studying laser-driven nuclear physics, is expected to produce high-intensity lasers with an intensity of 10^{25} W/cm^2 and peak power of 200 PW [11,12]. This will provide a unique opportunity for high-intensity laser-assisted nuclear decay.

Recent years witnessed significant progress in studying α decay and proton radioactivity [13–19]. Historically, modern theoretical nuclear physics originated from the explanation of α decay by Gamow, Gurney, and Condon in 1928 [20,21]. The α decay and proton radioactivity of atomic nuclei are fundamental decay modes of nuclei, providing important information about the nuclear structure [22–27]. The ultra-high-intensity laser electromagnetic fields have provided a new tool to explore firmly bound nuclear matter. Recently, many efforts have been dedicated to discussing the extent

to which high-intensity lasers can interfere with the half-life of the natural decay of atomic nuclei [11,28–34]. In fact, the electric-dipole term: $-Z_{\text{eff}}rE(t)\cos\theta$ determines the influence of high-intensity laser on nuclear decay, where r represents the mass center distance between the emitted proton and daughter nucleus. Compared with the α decay, the proton radioactivity of the nucleus has a larger r , which is more sensitive to the laser electric field. The study of the effect of laser on nuclear decay half-life depends on the calculation method of nuclear decay half-life. Recently, Delion *et al.* applied the Kramers-Henneberger approximation to the laser-assisted α decay process, which shows a result not in line with reality [30]. Therefore, there is a necessity to use a model that can accurately calculate the proton radioactivity half-life for analyzing the rate of change of the proton radioactivity half-life in a high-intensity laser field.

The laser-nucleus interaction introduces a new electric-dipole term in the nuclear Hamiltonian, which is closely related to the angle between the vector $\vec{E}(t)$ and the vector \vec{r} . Therefore, the influence of the deformation of the nucleus on proton radioactivity half-lives must be considered. This is not only for pursuing a better accurate calculation but also for obtaining a more microscopic understanding of the effect of the laser on proton radioactivity. Nowadays, many theoretical methods are used to study the α decay or proton radioactivity of deformed nuclei, including the deformed version of the density-dependent cluster model (DDCM) with microscopic double-folding potentials [35–37], the deformed Woods-Saxon (WS) potential [38–40], the deformed Cosh potentials [41], and others [26,42]. These calculation methods restore the potential of the emitted particles in the deformed nucleus to varying degrees. In the present work, we systematically study the rate of change of the proton radioactivity half-life of deformed proton emitters with $53 \leq Z \leq 83$ by using the state-of-the-art laser. The emitted proton-daughter

*tongpu@nudt.edu.cn

nucleus Coulomb potential is obtained by the double-folding model [35], and we have selected the classic cosh type [43] and Woods-Saxon nuclear potential [44], respectively. In addition, we found the nucleus with the most significant rate of change and investigated the relationship between the released energy of proton radioactivity and the maximum instantaneous rate of change of the proton radioactivity penetration probability. Moreover, we propose a method to increase the average rate of change in penetration probability, equivalent to increasing the laser intensity by two orders of magnitude.

This article is organized as follows. In the next section, the theoretical framework for the calculation of the proton radioactivity half-life and the parameters of a high-intensity Gaussian laser are described in detail. In Sec. III, the detailed calculations and discussions are provided. In Sec. IV, a brief summary is given.

II. THEORETICAL FRAMEWORK

A. The theoretical method

Proton radioactivity is an important decay mode for intermediate-mass nuclei. Its half-life can be written as [45]

$$T_{\frac{1}{2}} = \frac{\hbar \ln 2}{\Gamma}, \quad (1)$$

where \hbar is the reduced Planck constant, Γ is the proton radioactivity width depending on the proton collision probability, the formation probability, and the penetration probability. In the DDCM, the proton radioactivity width can be written as [35]

$$\Gamma = S_p \frac{\hbar^2}{4\mu} F P, \quad (2)$$

where S_p is the formation probability of the proton radioactivity, $\mu = \frac{M_d M_p}{M_d + M_p}$ is the reduced mass of the daughter nucleus, and the proton in the center-of-mass coordinate with M_p and M_d being masses of proton and the daughter nucleus, respectively. F is the normalized factor, describing the assault frequency, which is given by the integration over the internal region. Considering the influence of deformation, we obtain the total normalized factor F by averaging F_φ in all directions, which can be written as [35]

$$F = \frac{1}{2} \int_0^\pi F_\varphi \sin \varphi d\varphi, \quad (3)$$

$$F_\varphi = \frac{1}{\int_{R_1}^{R_2} \frac{1}{2k(r, t, \varphi, \theta)} dr}, \quad (4)$$

where φ is the orientation angle of the emitted proton with respect to the symmetry axis of the daughter nucleus. $k(r, t, \varphi, \theta)$ is the wave number, which can be written as

$$k(r, t, \varphi, \theta) = \sqrt{\frac{2\mu}{\hbar^2} |V(r, t, \varphi, \theta) - E_p|}, \quad (5)$$

where $V(r, t, \varphi, \theta)$ is the total interaction potential between the emitted proton and the daughter nucleus. The kinetic energy E_p of the emitted proton is determined by the released

energy of proton radioactivity Q_p , which can be given by

$$E_p = Q_p \frac{M_d}{M_d + M_p}. \quad (6)$$

For proton emission energy Q_p , we use the simple power-law interpolation for considering the overlapping effects on the half-lives of the proton emitters [46]. It is given by

$$Q_p = \Delta M - (\Delta M_d + \Delta M_p) + k(Z^\epsilon - Z_d^\epsilon), \quad (7)$$

where Z and Z_d are the proton numbers of the parent nuclei and daughter nucleus, respectively. The ΔM , ΔM_d , and ΔM_p are the mass excesses of the parent nucleus, daughter nucleus, and the emitted proton, respectively. The screening effect of the atomic electrons is represented by the term $k(Z^\epsilon - Z_d^\epsilon)$, for $Z < 60$, $k = 13.6$ eV, $\epsilon = 2.408$, and for $Z \geq 60$, $k = 8.7$ eV, $\epsilon = 2.517$ [47,48].

The classical turning point R_1 , R_2 , and the following R_3 are determined by the condition $V(r, t, \varphi, \theta) = E_p$. The penetration probability P as given in Eq. (2) can be obtained by the semiclassical Wentzel-Kramers-Brillouin (WKB) approximation. Considering the influence of deformation, we obtain the total penetration probability P by averaging P_φ in all directions, which can be written as [35]

$$P = \frac{1}{2} \int_0^\pi P_\varphi \sin \varphi d\varphi, \quad (8)$$

$$P_\varphi = \exp \left[-2 \int_{R_2}^{R_3} k(r, t, \varphi, \theta) dr \right]. \quad (9)$$

In this work, the total interaction potential $V(r, t, \varphi, \theta)$ between the emitted proton and the daughter nucleus is given by

$$V(r, t, \varphi, \theta) = \lambda(\varphi) V_N(r, \varphi) + V_l(r) + V_C(r, \varphi) + V_i(r, t, \theta). \quad (10)$$

$V_i(r, t, \theta)$ describes the interaction of the decaying system with the electromagnetic field [29]. More detailed information has been given in the next subsection. Here, $\lambda(\varphi)$ can be determined by using the Bohr-Sommerfeld quantization condition. $V_N(r, \varphi)$, $V_C(r, \varphi)$, and $V_l(r)$ represent the nuclear, Coulomb, and centrifugal potentials, respectively. In the present work, $V_l(r)$ is chosen as the Langer modified form [49]. It can be written as

$$V_l(r) = \frac{\hbar^2 \left(l + \frac{1}{2} \right)^2}{2\mu r^2}. \quad (11)$$

The Coulomb potential is obtained by the double-folding model, which can be expressed as

$$V_C(\vec{r}, \varphi) = \iint \frac{\rho_d(\vec{r}_1) \rho_p(\vec{r}_2)}{|\vec{r} + \vec{r}_2 - \vec{r}_1|} d\vec{r}_1 d\vec{r}_2, \quad (12)$$

where \vec{r} is the vector between the centers of the the emitted proton and daughter nucleus, \vec{r}_1 and \vec{r}_2 are the radius vectors in the charge distributions of the emitted proton and daughter nuclei. ρ_d and ρ_p are the density distribution of the daughter nucleus and proton, respectively. Simplified appropriately by the Fourier transform [50–52], the Coulomb potential can be approximated as

$$V_C(\vec{r}, \varphi) = V_C^{(0)}(\vec{r}, \varphi) + V_C^{(1)}(\vec{r}, \varphi) + V_C^{(2)}(\vec{r}, \varphi), \quad (13)$$

where $V_C^{(0)}(\vec{r}, \varphi)$, $V_C^{(1)}(\vec{r}, \varphi)$, and $V_C^{(2)}(\vec{r}, \varphi)$ are the bare Coulomb interaction, linear Coulomb coupling, and second-order Coulomb coupling, respectively [50].

The emitted proton-daughter nucleus nuclear potential $V_N(r, \varphi)$ was chosen as the classic cosh type [43] and Woods-Saxon (WS) [39] nuclear potential in this work. Since the nuclear potential is usually expressed in different forms in different studies [16,35,39,43], by comparing the calculation results obtained from different nuclear potentials, the effect of the laser on the half-life of proton radioactivity can be more accurately reflected. For a cosh type nuclear potential, it can be expressed as

$$V_N(r, \varphi) = -V_{01} \frac{1 + \cosh(R_d(\varphi)/a_1)}{\cosh(r/a_1) + \cosh(R_d(\varphi)/a_1)}, \quad (14)$$

where V_{01} and a_1 are the parameters of the depth and diffuseness of the nuclear potential, respectively. By considering the deformations, the $R_d(\varphi)$ is given by

$$R_d(\varphi) = R'_d(1 + \beta_2 Y_{20}(\varphi) + \beta_4 Y_{40}(\varphi) + \beta_6 Y_{60}(\varphi)), \quad (15)$$

where $Y_{ml}(\varphi)$ is a spherical harmonics function, β_2 , β_4 , and β_6 , respectively, denote the calculated quadrupole, hexadecapole, and hexacontatetrapole deformation of the nuclear ground state, which are taken from FRDM2012 [53]. R'_d is the spherical radius of the daughter nucleus, which can be expressed as

$$R'_d = 1.28A_d^{1/3} - 0.67 + 0.8A_d^{-1/3}, \quad (16)$$

where A_d is the mass number of the daughter nucleus.

For WS form, the nuclear potential is approximated as axially deformed [39], and it can be written as

$$V_N(r, \varphi) = \frac{V_{02}}{1 + \exp[(r - R_d(\varphi))/a_2]} \quad (17)$$

with $R_d(\varphi) = r_0 A_d^{1/3} (1 + \beta_2 Y_{20}(\varphi) + \beta_4 Y_{40}(\varphi) + \beta_6 Y_{60}(\varphi))$. The radius r_0 and the diffuseness a have the isospin-dependent form $r_0 = b + cI_d$, $a_2 = m + nI_d$ with $I_d = (N_d - Z_d)/A_d$. Here, N_d is the neutron number of the daughter nucleus. b , c , m , and n are adjustable parameters.

B. Laser-nucleus interaction

The effect of the laser electric field on the nucleus is determined by the electric-dipole term, which can be defined as [29]

$$V_i(\vec{r}, t, \theta) = -Z_{\text{eff}} \vec{r} \cdot \vec{E}(t) = -Z_{\text{eff}} r E(t) \cos \theta, \quad (18)$$

where θ is the angle between the vector $\vec{E}(t)$ and the vector \vec{r} . The effective charge Z_{eff} describes the tendency of the laser electric field to separate the emitted proton from the daughter nuclei, which can be written as

$$Z_{\text{eff}} = \frac{Z_p A_d - Z_d A_p}{A_d + A_p}, \quad (19)$$

where A_p and Z_p are the mass number and proton number of the emitted proton, respectively. If the daughter nucleus and the emitted proton have the same charge-to-mass ratio, they will move cooperatively in the laser field, and the laser electric field does not separate the two particles.

In this work, we assume a linear polarized Gaussian plane wave with the laser electric field,

$$E(t) = E_0 f(t) \sin(\omega t), \quad (20)$$

where E_0 and ω are the peak of the laser electric field and angular frequency, respectively. Here, E_0 depends on the peak of laser intensity I_0 , which can be written as [11]

$$E_0 [\text{Vcm}^{-1}] = \left(\frac{2I_0}{c\epsilon_0} \right)^{1/2} = 27.44 (I_0 [\text{Wcm}^{-2}])^{1/2}, \quad (21)$$

where c and ϵ_0 are the speed of light in vacuum and the permittivity of free space, respectively. $f(t)$ is the pulse shape function of a temporal profile. For simplicity, it is selected as square pulses in most recent theoretical studies [11,29,30,33,34]. The sequence of square pulses with an envelope function can be expressed as

$$f(t) = \sum_{j=1}^N (-1)^j \theta(t - \tau_j), \quad (22)$$

where τ_j is the duration of a single long pulse with constant amplitude, which makes the laser pulses act in the time intervals $\tau_0 = [0, \tau_1]$, $[\tau_2, \tau_3]$, etc.

However, the high-energy laser pulse delivered in the laboratory usually appears in a form of Gaussian shape [9,10]. The sequence of Gaussian pulses with an envelope function can be written as

$$f(t) = \exp\left(-\frac{t^2}{\tau^2}\right), \quad (23)$$

where the pulse width of the envelope $\tau = xT_0$ and T_0 is the pulse period. For femtosecond pulse, we choose to use phase $f(p = \omega t)$ instead of time $f(t)$ as the independent variable of the waveform function to improve the accuracy of the calculation in this work. Thus, it can be expressed as

$$f(t) = \exp\left(-\frac{t^2}{x^2 T_0^2}\right) = \exp\left(-\frac{p^2}{x^2 \omega^2 T_0^2}\right) = f(p), \quad (24)$$

where the pulse period $T_0 = 1/\nu$ and $\nu = \omega/2\pi$ is the frequency. Equation (24) can be simplified to

$$f(p) = \exp\left(-\frac{p^2}{4\pi^2 x^2}\right). \quad (25)$$

In principle, the kinetic energy of the emitted proton should also be changed by the laser fields. The changed kinetic energy is equal to the energy of the protons accelerated by the laser electric field obtained by the emitted protons inside the nucleus. Equation (6) can thus be rewritten as

$$E_p = Q_p \frac{M_d}{M_d + M_p} + eE(t)R'_d \cos \theta. \quad (26)$$

In this framework, the total emitted proton-daughter nucleus interaction potential $V(r, p, \varphi, \theta)$ is shown in Fig. 1. Here, the red curve and the black curve represent $V(r, p, \varphi, \theta) = V(r, \varphi) + V_i(r, p, \theta)$ and $V(r, \varphi)$ without the laser electric field, respectively. E_p^* and R_i^* ($i = 1, 2, 3$) correspond to the kinetic energy and classical turning point considering the laser electric field. E_p and R_i ($i = 1, 2, 3$) refer to the kinetic energy and classical turning point without the laser electric field.

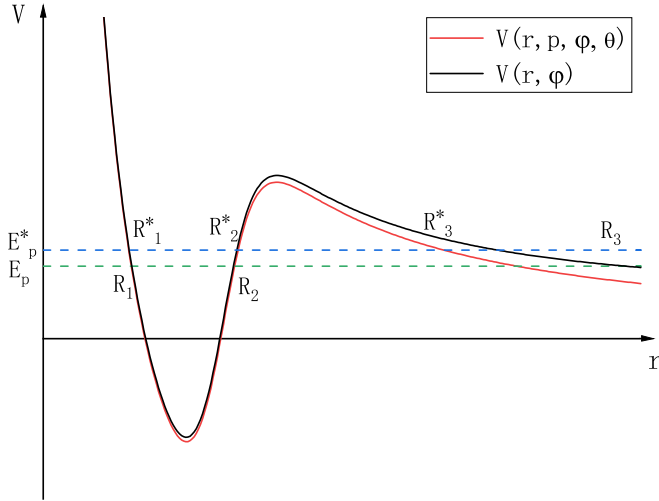


FIG. 1. Schematic diagram of the total potential $V(r, p, \varphi, \theta)$. The red curve and the black curve represent $V(r, p, \varphi, \theta) = V(r, \varphi) + V_i(r, p, \theta)$ and $V(r, \varphi)$ without the laser electric field, respectively. E_p^* and R_i^* ($i = 1, 2, 3$) correspond to the kinetic energy and classical turning point considering the laser electric field. E_p and R_i ($i = 1, 2, 3$) refer to the kinetic energy and classical turning point without the laser electric field.

III. RESULTS AND DISCUSSION

A. Gaussian laser-assisted proton radioactivity

In the present work, the least-squares principle is used to refit the adjustable parameters, we determined the parameters of cosh type and WS nuclear potential, i.e., the depth V_0 and diffuseness a of the nuclear potential while $S_p = S_0 = 0.5$ is an approximation taken from Ref. [54]. The experimental data of parity, spin, proton radioactivity half-lives, and the proton radioactivity energy Q_p are taken from the latest evaluated atomic mass table AME2020 [55,56] and the latest evaluated nuclear properties table NUBASE2020 [57] except for those of ^{144}Tm , ^{151}Lu , ^{159}Re , and ^{164}Ir , which are taken from Ref. [58]. The standard deviation σ indicates the divergence between the theoretical proton radioactivity half-lives and the experimental ones, which can be expressed as $\sigma = \sqrt{\sum (lgT_{1/2}^{\text{exp}}(s) - lgT_{1/2}^{\text{cal}}(s))^2/n}$. In the case of $V_i(r, p, \theta) = 0$, the slightest standard deviation and the values of adjustable parameters are given as

$$V_{01} = 57.83 \text{ MeV}, \quad a_1 = 0.857 \text{ fm}. \quad (27)$$

$$V_{02} = 52.44 \text{ MeV}, \quad b = 1.27, \quad c = 1.70,$$

$$m = 0.113, \quad n = 0.685. \quad (28)$$

The results $\sigma_{\text{cosh}} = 0.588$ and $\sigma_{\text{WS}} = 0.511$ represent standard deviations between $lgT_{1/2}^{\text{cosh}}$, $lgT_{1/2}^{\text{WS}}$, and $lgT_{1/2}^{\text{exp}}$, respectively. The detailed results are listed in Table I. In this table, the first six columns represent the parent nuclei, the orbital angular momentum l taken away by the emitted proton, the kinetic energy of the emitted proton E_p , the logarithmic form of the experimental proton radioactivity half-lives, the logarithmic

form of the theoretical proton radioactivity half-lives calculated by the cosh type and WS nuclear potential, respectively. This table shows that the theoretical proton radioactivity half-lives can reproduce the experimental data well. Moreover, we also found that the calculations by using the WS nuclear potential can better reproduce the experimental data than the cosh type nuclear potential for most parent nuclei. Therefore, it is credible to study the effect of the laser field on the proton radioactivity half-life based on the WS nuclear potential and we choose the WS nuclear potential for calculation in the following work.

At present, the high-intensity laser pulse based on chirped pulse amplification technique can be realized, and the peak intensity exceeds 10^{23} W/cm^2 [10]. Its full width at half-maximum (FWHM) is approximately $19.6 \text{ fs} (= 1.96 \times 10^{-14} \text{ s})$. For proton radioactivity, the emitted protons oscillate back and forth within the nucleus at high frequencies, and we may estimate how much time the emitted protons need to tunnel through the potential barrier. The range of the potential barrier for the emitted protons to tunnel through is $0 < R_d < 10$ (fm). The emitted protons need about $5 \times 10^{-20} \text{ s}$ to travel through the potential barrier. An optical cycle of strong lasers is much longer than this time. Therefore, the process of emitted protons penetrating through the potential barrier is regarded as the quasistatic approximation. In this case, the change of the laser field is negligible. This approximation is usually used to describe the tunneling ionization of atoms in strong-field atomic physics [59,60]. As shown in Table I, the kinetic energy of the emitted protons is more diminutive than 2 MeV. One gets the emitted proton's speed, which is smaller than $2 \times 10^7 \text{ m/s}$. So the emitted protons move much slower than the speed of light. It means that the effect of the laser electric field on the emitted protons is expected to be much greater than the laser magnetic field. Therefore, we can ignore the magnetic part of the laser field in this situation. Moreover, the assault frequency is determined by the principal quantum number G [61], thus we assume that the strong external laser fields mainly affect the half-life of proton radioactivity by modifying the proton radioactivity penetration probability. For interpretation, we first define the rate of change of penetration probability ΔP and the rate of change of proton radioactivity half-life ΔT ,

$$\Delta P = \frac{P(E, \theta) - P(E = 0, \theta)}{P(E = 0, \theta)}, \quad (29)$$

$$\Delta T = \frac{T(E, \theta) - T(E = 0, \theta)}{T(E = 0, \theta)}, \quad (30)$$

and we can get

$$\Delta T = \frac{P(E = 0, \theta) - P(E, \theta)}{P(E, \theta)}. \quad (31)$$

The laser field may also change the preformation probability of the proton-daughter nucleus configuration in the parent nucleus. The experimental formation probability of proton radioactivity can be extracted from ratios of calculated proton radioactivity half-life $T_{1/2}^{\text{cal}}$ to experimental data $T_{1/2}^{\text{exp}}$, which is defined as $S_p = S_0 T_{1/2}^{\text{cal}}/T_{1/2}^{\text{exp}}$. Both the semimicroscopic

TABLE I. Comparison between the experimental data and calculated half-lives of proton radioactivity. lgT_{cal1} and lgT_{cal2} represent the theoretical half-lives of proton radioactivity calculated by the cosh type and WS nuclear potential, respectively. ΔP_1 and ΔT_1 is calculated by the cosh type nuclear potential in the case of the laser intensity of 10^{23} W/cm². ΔP_2 and ΔT_2 calculated by the WS type nuclear potential in the case of the laser intensity of 10^{23} W/cm².

Nucleus	l	E_p (MeV)	Measured (s)	lgT_{cal1} (s)	lgT_{cal2} (s)	ΔP_1	ΔT_1	ΔP_2	ΔT_2
¹⁰⁸ I	2	0.6	0.723	0.018	0.523	2.76×10^{-3}	-2.75×10^{-3}	2.64×10^{-3}	-2.63×10^{-3}
¹⁰⁹ I	0	0.821	-4.032	-5.123	-4.589	1.34×10^{-3}	-1.34×10^{-3}	1.21×10^{-3}	-1.20×10^{-3}
¹¹² Cs	2	0.818	-3.31	-3.323	-2.884	1.35×10^{-3}	-1.35×10^{-3}	1.34×10^{-3}	-1.34×10^{-3}
¹¹³ Cs	2	0.973	-4.771	-5.509	-5.08	9.23×10^{-4}	-9.22×10^{-4}	8.43×10^{-4}	-8.42×10^{-4}
¹¹⁷ La	2	0.823	-1.664	-2.738	-2.345	1.41×10^{-3}	-1.41×10^{-3}	1.47×10^{-3}	-1.47×10^{-3}
¹²¹ Pr	2	0.893	-1.921	-3.078	-2.775	1.32×10^{-3}	-1.32×10^{-3}	1.31×10^{-3}	-1.31×10^{-3}
¹³¹ Eu	2	0.951	-1.699	-2.528	-2.334	1.29×10^{-3}	-1.29×10^{-3}	1.27×10^{-3}	-1.27×10^{-3}
¹³⁵ Tb	3	1.191	-2.996	-3.956	-3.875	7.61×10^{-4}	-7.60×10^{-4}	7.96×10^{-4}	-7.96×10^{-4}
¹⁴¹ Ho ^m	0	1.251	-5.137	-5.694	-5.443	-3.93×10^{-3}	3.95×10^{-3}	6.28×10^{-4}	-6.27×10^{-4}
¹⁴¹ Ho	3	1.181	-2.387	-3.236	-3.261	9.34×10^{-4}	-9.33×10^{-4}	8.51×10^{-4}	-8.50×10^{-4}
¹⁴⁴ Tm	5	1.726	-5.569	-4.843	-5.518	3.33×10^{-4}	-3.33×10^{-4}	3.56×10^{-4}	-3.56×10^{-4}
¹⁴⁵ Tm	5	1.737	-5.499	-4.941	-5.566	4.42×10^{-4}	-4.42×10^{-4}	3.68×10^{-4}	-3.68×10^{-4}
¹⁴⁶ Tm ^m	5	1.211	-1.137	-0.54	-1.206	9.10×10^{-4}	-9.09×10^{-4}	8.96×10^{-4}	-8.95×10^{-4}
¹⁴⁶ Tm	0	0.903	-0.81	-0.502	-0.275	1.78×10^{-3}	-1.77×10^{-3}	1.66×10^{-3}	-1.66×10^{-3}
¹⁴⁷ Tm	5	1.065	0.587	1.297	0.605	1.15×10^{-3}	-1.15×10^{-3}	1.17×10^{-3}	-1.17×10^{-3}
¹⁴⁷ Tm ^m	2	1.126	-3.444	-2.885	-2.755	1.02×10^{-3}	-1.02×10^{-3}	1.04×10^{-3}	-1.04×10^{-3}
¹⁵⁰ Lu ^m	2	1.295	-4.398	-4.335	-4.048	7.82×10^{-4}	-7.82×10^{-4}	7.27×10^{-4}	-7.26×10^{-4}
¹⁵⁰ Lu	5	1.275	-1.347	-0.769	-0.998	9.23×10^{-4}	-9.22×10^{-4}	7.61×10^{-4}	-7.61×10^{-4}
¹⁵¹ Lu ^m	2	1.306	-4.796	-4.463	-4.214	7.79×10^{-4}	-7.79×10^{-4}	6.85×10^{-4}	-6.84×10^{-4}
¹⁵¹ Lu	5	1.261	-0.896	-0.609	-0.873	8.08×10^{-4}	-8.07×10^{-4}	8.85×10^{-4}	-8.84×10^{-4}
¹⁵⁵ Ta	5	1.458	-2.495	-2.037	-2.231	7.35×10^{-4}	-7.34×10^{-4}	6.63×10^{-4}	-6.62×10^{-4}
¹⁵⁶ Ta	2	1.028	-0.826	-0.44	-0.227	1.31×10^{-3}	-1.31×10^{-3}	1.40×10^{-3}	-1.40×10^{-3}
¹⁵⁶ Ta ^m	5	1.117	0.933	1.645	1.346	1.25×10^{-3}	-1.25×10^{-3}	1.20×10^{-3}	-1.20×10^{-3}
¹⁵⁷ Ta	0	0.944	-0.527	0.089	0.358	1.69×10^{-3}	-1.68×10^{-3}	1.74×10^{-3}	-1.74×10^{-3}
¹⁵⁹ Re ^m	5	1.805	-4.665	-4.24	-4.45	4.23×10^{-4}	-4.23×10^{-4}	3.95×10^{-4}	-3.95×10^{-4}
¹⁵⁹ Re	5	1.82	-4.678	-4.374	-4.577	3.92×10^{-4}	-3.92×10^{-4}	3.71×10^{-4}	-3.71×10^{-4}
¹⁶⁰ Re	0	1.274	-3.163	-3.716	-3.447	9.99×10^{-4}	-9.98×10^{-4}	9.20×10^{-4}	-9.19×10^{-4}
¹⁶¹ Re ^m	5	1.324	-0.678	-0.247	-0.629	9.06×10^{-4}	-9.05×10^{-4}	9.43×10^{-4}	-9.42×10^{-4}
¹⁶¹ Re	0	1.205	-3.306	-2.904	-2.654	9.66×10^{-4}	-9.65×10^{-4}	1.04×10^{-3}	-1.04×10^{-3}
¹⁶⁴ Ir	5	1.848	-3.959	-4.134	-4.387	4.91×10^{-4}	-4.90×10^{-4}	4.30×10^{-4}	-4.30×10^{-4}
¹⁶⁵ Ir ^m	5	1.716	-3.433	-3.215	-3.57	4.67×10^{-4}	-4.67×10^{-4}	5.50×10^{-4}	-5.50×10^{-4}
¹⁶⁶ Ir	2	1.161	-0.824	-1.054	-0.894	1.11×10^{-3}	-1.10×10^{-3}	1.15×10^{-3}	-1.14×10^{-3}
¹⁶⁶ Ir ^m	5	1.34	-0.076	0.089	-0.342	8.97×10^{-4}	-8.97×10^{-4}	1.02×10^{-3}	-1.02×10^{-3}
¹⁶⁷ Ir	0	1.079	-1.12	-0.705	-0.51	1.36×10^{-3}	-1.35×10^{-3}	1.40×10^{-3}	-1.40×10^{-3}
¹⁶⁷ Ir ^m	5	1.253	0.842	1.045	0.542	9.45×10^{-4}	-9.44×10^{-4}	1.15×10^{-3}	-1.15×10^{-3}
¹⁷⁰ Au	2	1.48	-3.487	-3.921	-3.773	6.77×10^{-4}	-6.77×10^{-4}	6.91×10^{-4}	-6.90×10^{-4}
¹⁷⁰ Au ^m	5	1.758	-3.975	-3.078	-3.469	5.21×10^{-4}	-5.21×10^{-4}	5.03×10^{-4}	-5.03×10^{-4}
¹⁷¹ Au ^m	5	1.708	-2.587	-2.719	-3.196	3.96×10^{-4}	-3.96×10^{-4}	6.15×10^{-4}	-6.15×10^{-4}
¹⁷¹ Au	0	1.456	-4.652	-4.489	-4.24	6.64×10^{-4}	-6.64×10^{-4}	6.90×10^{-4}	-6.90×10^{-4}
¹⁷⁶ Tl	0	1.275	-2.208	-1.996	-1.896	9.83×10^{-4}	-9.82×10^{-4}	9.58×10^{-4}	-9.57×10^{-4}
¹⁷⁷ Tl ^m	5	1.969	-3.346	-4.131	-4.668	4.13×10^{-4}	-4.13×10^{-4}	3.77×10^{-4}	-3.77×10^{-4}
¹⁷⁷ Tl	0	1.182	-1.178	-0.865	-0.752	1.15×10^{-3}	-1.15×10^{-3}	1.28×10^{-3}	-1.28×10^{-3}
¹⁸⁵ Bi ^m	0	1.616	-4.191	-4.901	-4.843	6.56×10^{-4}	-6.56×10^{-4}	6.32×10^{-4}	-6.32×10^{-4}

method and the phenomenological method are used to calculate the probability of formation of proton radioactivity [62–65]. In the present work, the rate of change of the formation probability ΔS_p is defined as

$$\Delta S_p = \frac{S_p(E = 0, \theta) - S_p(E, \theta)}{S_p(E, \theta)}. \quad (32)$$

In addition, we calculate the influence of a peak intensity of 10^{23} W/cm² laser pulse on proton radioactivity in Table I. In

this table, the seventh and eighth columns present ΔT_1 , ΔP_1 calculated by the cosh type nuclear potential in the case of peak laser intensity $I_0 = 10^{23}$ W/cm² and $\theta = 0$, respectively. And the last two columns represent the columns present ΔT_2 , ΔP_2 calculated by the WS nuclear potential in the case of peak laser intensity $I_0 = 10^{23}$ W/cm² and $\theta = 0$, respectively. As seen from this table, ΔT and ΔP for different parent nuclei have different sensitivities to the laser with an intensity of 10^{23} W/cm². They range from 0.01% to 0.3%, and the most sensitive parent nuclei to the high-intensity laser are ¹⁰⁸I.

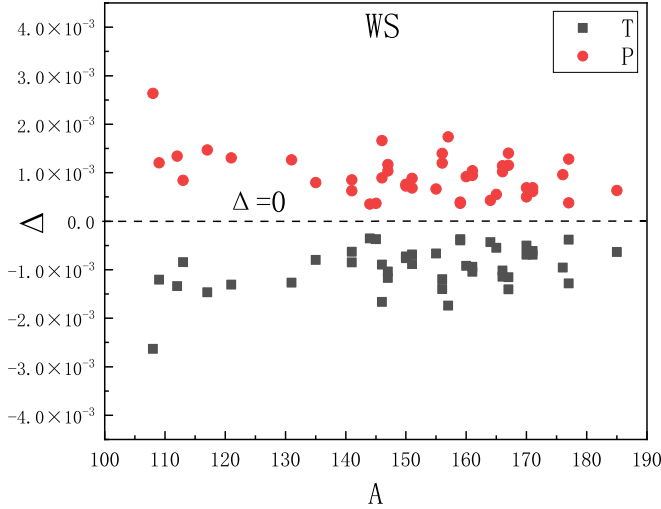


FIG. 2. The rate of the change of penetration probability and the rate of the change of proton radioactivity half-life for different parent nuclei have different sensitivity to the high-intensity laser with an intensity of 10^{23} W/cm². The black square and the red circle represent ΔT and ΔP , respectively.

Moreover, ΔS_p changes according to the changes of ΔT and the rate of change of penetration probability of most nuclei shows uniformity. It can be seen from Fig. 1 that due to the addition of the laser field, the distance between R_2 and R_3 becomes smaller, and the total potential barrier is reduced, increasing the proton radioactivity penetration probability.

To intuitively compare the rate of the change of penetration probability and the rate of the change of proton radioactivity half-life for different parent nuclei, ΔT_2 and ΔP_2 from Table I are shown in Fig. 2. In this figure, the x axis represents the mass number of the parent nuclei, the black square and the red circle represent ΔT_2 and ΔP_2 , respectively. From Fig. 2, we can clearly see that the most sensitive parent nuclei to the high-intensity laser is ^{108}I . In addition, for the identical parent nuclei, ΔT_2 and ΔP_2 seem to be symmetrical about $\Delta = 0$.

With the same intensity of the laser pulse and θ as in Fig. 2, Fig. 3 shows that ΔT and ΔP of ^{108}I oscillate in a Gaussian laser electric field in the case of $\tau = 3T_0$. In this figure, the x axis represents the phase of the laser pulse, the y axis represents the rate of change of proton radioactivity half-life or penetration probability. The schematic diagram of the laser electric field waveform is in the red box in the upper left corner of this figure. The black curve and green curve represent ΔP and ΔT for ^{108}I , respectively. This figure shows that ΔP and ΔT are symmetric about $\Delta = 0$. To interpret this result, we set $P'(E, \theta) = P(E, \theta) - P(E = 0, \theta)$ and substitute it into Eq. (31), thus we obtain

$$\Delta T = -\frac{P'(E, \theta)}{P'(E, \theta) + P(E, \theta)}. \quad (33)$$

For $P'(E, \theta) \ll P(E, \theta)$, Eq. (31) can be written as

$$\Delta T \approx -\frac{P'(E, \theta)}{P(E, \theta)} = -\Delta P. \quad (34)$$

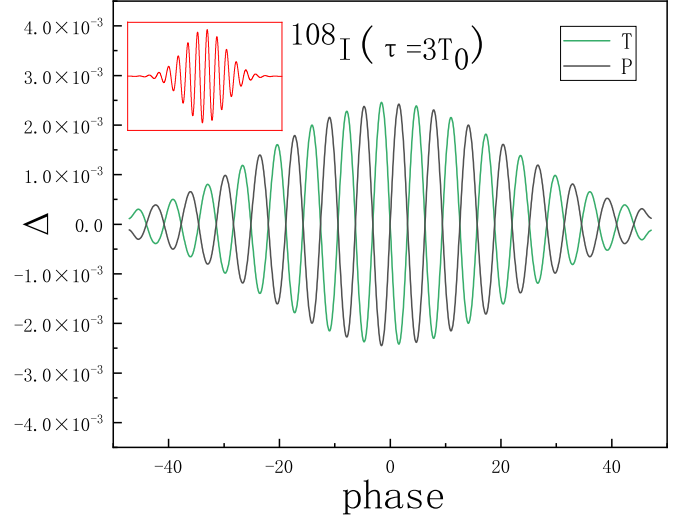


FIG. 3. ΔT and ΔP of ^{108}I oscillate with a Gaussian laser electric field.

Once the laser intensity is large enough, this approximation fails, and the symmetry of ΔP and ΔT will be broken. Compared to the laser potential at the laser intensity of 10^{23} W/cm², the potential between the emitted protons and the daughter nucleus is several orders of magnitudes higher. Therefore, the laser potential can be regarded as a perturbation to the emitted protons-nucleus potential. To explain more clearly the influence of laser disturbance on ΔP , ΔT and the symmetry between ΔP and ΔT , we start from the penetrability probability given by Eq. (9) and write it in the following form:

$$P_\varphi(r, p, \theta) = \exp\left[-\frac{2(2\mu)^{1/2}}{\hbar} \int_{R_2}^{R_3} \sqrt{V_{\varphi ICN} \left(1 + \frac{V_i}{V_{\varphi ICN}}\right)} dr\right], \quad (35)$$

where $V_{\varphi ICN} = \lambda(\varphi)V_N(r, \varphi) + V_l(r) + V_C(r, \varphi) - E_p$ represents the integrand function without the laser modification. For $V_i \ll V_{\varphi ICN}$, we have the following Taylor expansion:

$$\begin{aligned} P_\varphi(r, p, \theta) &= \exp\left[-\frac{2(2\mu)^{1/2}}{\hbar} \int_{R_2}^{R_3} \sqrt{V_{\varphi ICN}} \right. \\ &\quad \left. \times \left(1 + \frac{V_i}{2V_{\varphi ICN}} + \frac{V_i^2}{8V_{\varphi ICN}^2} + \dots\right) dr\right] \\ &\approx \exp\left[-\frac{2(2\mu)^{1/2}}{\hbar} \int_{R_2}^{R_3} \sqrt{V_{\varphi ICN}} \right. \\ &\quad \left. \times \left(1 + \frac{V_i}{2V_{\varphi ICN}} + \frac{V_i^2}{8V_{\varphi ICN}^2}\right) dr\right] \\ &= \exp[\chi_\varphi^{(0)} + \chi_\varphi^{(1)} + \chi_\varphi^{(2)}] \\ &= \exp[\chi_\varphi^{(0)}] \exp[\chi_\varphi^{(1)} + \chi_\varphi^{(2)}], \end{aligned} \quad (36)$$

where $\chi_\varphi^{(0)}$, $\chi_\varphi^{(1)}$, and $\chi_\varphi^{(2)}$ can be expressed as

$$\chi_\varphi^{(0)} = -\frac{2(2\mu)^{1/2}}{\hbar} \int_{R_2}^{R_3} \sqrt{V_{\varphi ICN}} dr = P_\varphi(r, E = 0, \theta), \quad (37)$$

$$\chi_{\varphi}^{(1)} = e(p) \times \frac{(2\mu)^{1/2} Z_{\text{eff}} \cos \theta}{\hbar} \int_{R_2}^{R_3} \frac{r}{\sqrt{V_{\varphi|CN}}} dr, \quad (38)$$

$$\begin{aligned} \chi_{\varphi}^{(2)} &= e^2(p) \times \frac{(2\mu)^{1/2} (Z_{\text{eff}} \cos \theta)^2}{4\hbar} \int_{R_2}^{R_3} \frac{r^2}{V_{\varphi|CN}^{3/2}} dr \\ &= \frac{1}{c\epsilon_0} i(p) \times \frac{(2\mu)^{1/2} (Z_{\text{eff}} \cos \theta)^2}{2\hbar} \int_{R_2}^{R_3} \frac{r^2}{V_{\varphi|CN}^{3/2}} dr, \quad (39) \end{aligned}$$

where $P_{\varphi}(r, E = 0, \theta)$ represents the penetration probability for same φ without the laser modification. And $i(p)$ represents the laser field intensity, which is proportional to the square of the laser electric field intensity $e^2(p)$. The rate of change of penetration probability for the same φ can be rewritten as

$$\begin{aligned} \Delta P_{\varphi} &= \frac{\exp[\chi^{(0)}] \exp[\chi^{(1)} + \chi^{(2)}] - P_{\varphi}(r, E = 0, \theta)}{P_{\varphi}(r, E = 0, \theta)} \\ &= \exp[\chi_{\varphi}^{(1)} + \chi_{\varphi}^{(2)}] - 1. \quad (40) \end{aligned}$$

As $\chi_{\varphi}^{(1)} + \chi_{\varphi}^{(2)}$ approaches 0, $\exp[\chi_{\varphi}^{(1)} + \chi_{\varphi}^{(2)}]$ approaches $1 + \chi_{\varphi}^{(1)} + \chi_{\varphi}^{(2)}$, we can write Eq. (40) in the following form:

$$\Delta P_{\varphi} = \chi_{\varphi}^{(1)} + \chi_{\varphi}^{(2)}. \quad (41)$$

It can be seen that the proton radioactivity penetration probability for the same φ in a high-intensity laser field depends on the proton radioactivity penetration probability without the laser field $P_{\varphi}(r, E = 0, \theta)$, the laser electric field $e(p)$, and the laser field intensity $i(p)$. The total penetration probability P by averaging P_{φ} in all directions, so the main factor that affects the deviation of the penetration probability is the laser electric field $e(p)$ in a weak laser electric field. And $e(p)$ is symmetrical about $e(p) = 0$, so both ΔP and ΔT have $\Delta = 0$ symmetry in Fig. 3. When the laser electric field becomes large, this symmetry will be broken by the laser intensity $i(p)$.

To examine our conjecture, we calculate ΔP of ^{108}I , for four laser pulses with different peak intensities, namely, 10^{25} W/cm^2 , 10^{26} W/cm^2 , 10^{27} W/cm^2 , and 10^{28} W/cm^2 . The same τ and θ are used as in Fig. 2. The results are shown in Figs. 4 and 5, respectively. From these figures, we can find that as the laser intensity increases, the symmetry of ΔP and ΔT about the $\Delta = 0$ is gradually destroyed. In addition, for the same laser pulse, the maximum value of ΔP and ΔT will appear at the laser peak intensity. For ^{108}I , with the increase of laser peak intensity I_0 , the maximum value of ΔP and ΔT increase progressively to 1.2. It means the maximum instantaneous change of the proton radioactivity half-life will reach 120% in the high-intensity laser with the laser peak intensity at $I_0 = 10^{28} \text{ W/cm}^2$.

Under the influence of the laser field, the instantaneous rate of change of the penetration probability oscillates back and forth on the x axis as the phase changes. To obtain the total effect of a single laser pulse on the penetration probability, we calculate the average penetration probability of laser pulses with different peak intensities in Table II. The same τ and θ are used as in Fig. 2. In this table, the first column is the parent nuclei, and the following six columns represent the

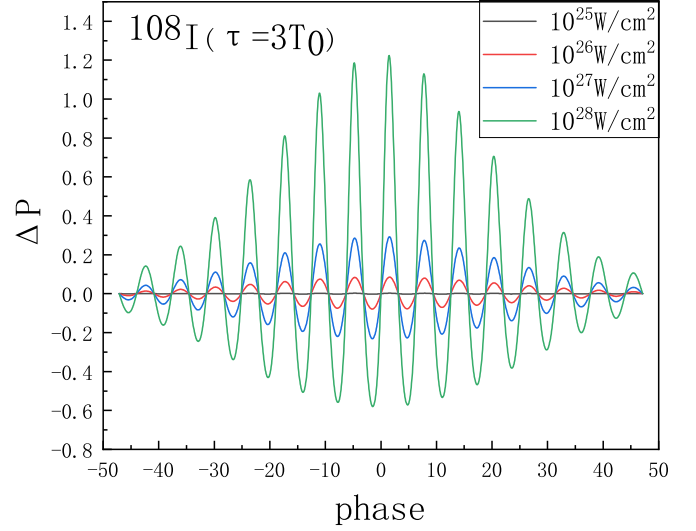


FIG. 4. ΔP for ^{108}I with $I_0 = 10^{25} \text{ W/cm}^2$, 10^{26} W/cm^2 , 10^{27} W/cm^2 , and 10^{28} W/cm^2 .

average value and the maximum value of ΔP in the case of $I_0 = 10^{23} \text{ W/cm}^2$, 10^{24} W/cm^2 , and 10^{25} W/cm^2 denoted as $\Delta P_{\text{avg}}^{23}$, $\Delta P_{\text{avg}}^{24}$, $\Delta P_{\text{avg}}^{25}$, $\Delta P_{\text{max}}^{23}$, $\Delta P_{\text{max}}^{24}$, and $\Delta P_{\text{max}}^{25}$.

From this table, we can clearly see that the average rate of change of proton radioactivity penetration probability may be positive or negative in the case of low laser intensity. This is the result of the laser electric field oscillating back and forth with the change of phase. As the laser intensity increases, the average rate of change of proton radioactivity penetration probability is uniformly positive, and this result is consistent with the conclusions in Figs. 4 and 5. Moreover, the average rate of change and the maximum instantaneous rate of change in the penetration probability of ^{108}I is the largest compared to other parent nuclei under any laser intensity aforementioned. Some recent studies have found that the decay energy

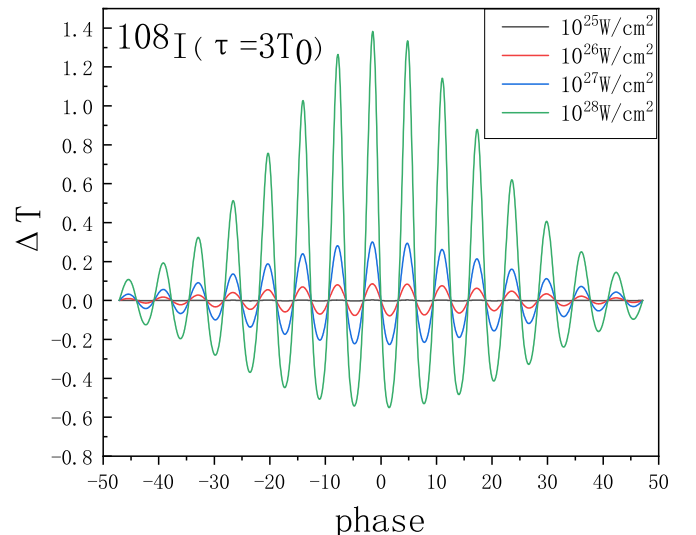


FIG. 5. ΔT for ^{108}I with $I_0 = 10^{25} \text{ W/cm}^2$, 10^{26} W/cm^2 , 10^{27} W/cm^2 , and 10^{28} W/cm^2 .

TABLE II. The calculation of the average value and the maximum value of ΔP in the case of $I_0 = 10^{23}$ W/cm², 10^{24} W/cm², and 10^{25} W/cm², respectively.

Nucleus	$\Delta P_{\text{avg}}^{23}$	$\Delta P_{\text{avg}}^{24}$	$\Delta P_{\text{avg}}^{25}$	$\Delta P_{\text{max}}^{23}$	$\Delta P_{\text{max}}^{24}$	$\Delta P_{\text{max}}^{25}$
¹⁰⁸ I	1.48×10^{-6}	8.72×10^{-6}	7.69×10^{-5}	2.64×10^{-3}	7.67×10^{-3}	2.38×10^{-2}
¹⁰⁹ I	1.73×10^{-6}	2.67×10^{-6}	1.72×10^{-5}	1.21×10^{-3}	3.47×10^{-3}	1.08×10^{-2}
¹¹² Cs	1.14×10^{-6}	3.09×10^{-6}	2.03×10^{-5}	1.34×10^{-3}	3.80×10^{-3}	1.18×10^{-2}
¹¹³ Cs	2.52×10^{-6}	1.87×10^{-6}	9.57×10^{-6}	8.43×10^{-4}	2.51×10^{-3}	7.78×10^{-3}
¹¹⁷ La	-1.53×10^{-6}	2.26×10^{-6}	2.43×10^{-5}	1.47×10^{-3}	4.15×10^{-3}	1.28×10^{-2}
¹²¹ Pr	-9.59×10^{-7}	1.03×10^{-6}	1.88×10^{-5}	1.31×10^{-3}	3.67×10^{-3}	1.11×10^{-2}
¹³¹ Eu	2.17×10^{-6}	1.22×10^{-6}	1.81×10^{-5}	1.27×10^{-3}	3.52×10^{-3}	1.09×10^{-2}
¹³⁵ Tb	-2.08×10^{-6}	-1.13×10^{-6}	4.93×10^{-6}	7.96×10^{-4}	2.25×10^{-3}	6.86×10^{-3}
¹⁴¹ Ho ^m	8.17×10^{-7}	7.61×10^{-7}	6.97×10^{-6}	6.28×10^{-4}	2.00×10^{-3}	6.16×10^{-3}
¹⁴¹ Ho	-6.97×10^{-7}	-6.75×10^{-7}	9.70×10^{-6}	8.51×10^{-4}	2.42×10^{-3}	7.42×10^{-3}
¹⁴⁴ Tm	-9.21×10^{-7}	8.62×10^{-7}	1.55×10^{-6}	3.56×10^{-4}	1.08×10^{-3}	3.34×10^{-3}
¹⁴⁵ Tm	1.88×10^{-6}	2.05×10^{-6}	1.78×10^{-6}	3.68×10^{-4}	1.06×10^{-3}	3.29×10^{-3}
¹⁴⁶ Tm ^m	2.41×10^{-6}	2.15×10^{-6}	9.54×10^{-6}	8.96×10^{-4}	2.59×10^{-3}	7.88×10^{-3}
¹⁴⁶ Tm	7.65×10^{-8}	2.67×10^{-6}	3.12×10^{-5}	1.66×10^{-3}	4.80×10^{-3}	1.49×10^{-2}
¹⁴⁷ Tm	-1.98×10^{-7}	5.09×10^{-6}	1.84×10^{-5}	1.17×10^{-3}	3.63×10^{-3}	1.09×10^{-2}
¹⁴⁷ Tm ^m	1.36×10^{-6}	2.77×10^{-6}	1.28×10^{-5}	1.04×10^{-3}	2.87×10^{-3}	8.76×10^{-3}
¹⁵⁰ Lu ^m	1.46×10^{-6}	1.34×10^{-6}	7.28×10^{-6}	7.27×10^{-4}	2.21×10^{-3}	6.52×10^{-3}
¹⁵⁰ Lu	3.33×10^{-6}	1.57×10^{-6}	7.89×10^{-6}	7.61×10^{-4}	2.29×10^{-3}	7.31×10^{-3}
¹⁵¹ Lu ^m	-3.94×10^{-6}	-1.17×10^{-7}	6.64×10^{-6}	6.85×10^{-4}	2.04×10^{-3}	6.45×10^{-3}
¹⁵¹ Lu	2.06×10^{-6}	-7.61×10^{-7}	8.64×10^{-6}	8.85×10^{-4}	2.54×10^{-3}	7.67×10^{-3}
¹⁵⁵ Ta	-6.95×10^{-7}	1.45×10^{-6}	5.53×10^{-6}	6.63×10^{-4}	1.83×10^{-3}	5.61×10^{-3}
¹⁵⁶ Ta	2.58×10^{-6}	4.29×10^{-6}	2.21×10^{-5}	1.40×10^{-3}	3.98×10^{-3}	1.24×10^{-2}
¹⁵⁶ Ta ^m	4.32×10^{-7}	6.42×10^{-7}	1.71×10^{-5}	1.20×10^{-3}	3.56×10^{-3}	1.08×10^{-2}
¹⁵⁷ Ta	4.99×10^{-7}	4.15×10^{-6}	3.41×10^{-5}	1.74×10^{-3}	4.97×10^{-3}	1.52×10^{-2}
¹⁵⁹ Re ^m	-1.08×10^{-6}	-1.33×10^{-6}	1.90×10^{-6}	3.95×10^{-4}	1.18×10^{-3}	3.51×10^{-3}
¹⁵⁹ Re	3.70×10^{-7}	9.32×10^{-7}	1.48×10^{-6}	3.71×10^{-4}	1.19×10^{-3}	3.49×10^{-3}
¹⁶⁰ Re	-8.32×10^{-7}	4.05×10^{-7}	9.50×10^{-6}	9.20×10^{-4}	2.48×10^{-3}	7.54×10^{-3}
¹⁶¹ Re ^m	1.45×10^{-6}	1.84×10^{-6}	8.13×10^{-6}	9.43×10^{-4}	2.51×10^{-3}	7.57×10^{-3}
¹⁶¹ Re	-4.28×10^{-7}	1.79×10^{-7}	1.19×10^{-5}	1.04×10^{-3}	2.92×10^{-3}	8.70×10^{-3}
¹⁶⁴ Ir	-1.97×10^{-6}	-9.54×10^{-7}	2.03×10^{-6}	4.30×10^{-4}	1.20×10^{-3}	3.57×10^{-3}
¹⁶⁵ Ir ^m	2.69×10^{-6}	-4.11×10^{-8}	3.36×10^{-6}	5.50×10^{-4}	1.45×10^{-3}	4.30×10^{-3}
¹⁶⁶ Ir	1.95×10^{-6}	1.86×10^{-6}	1.74×10^{-5}	1.15×10^{-3}	3.26×10^{-3}	1.02×10^{-2}
¹⁶⁶ Ir ^m	3.27×10^{-7}	1.32×10^{-6}	8.35×10^{-6}	1.02×10^{-3}	2.60×10^{-3}	7.79×10^{-3}
¹⁶⁷ Ir	5.59×10^{-7}	3.48×10^{-6}	2.18×10^{-5}	1.40×10^{-3}	4.01×10^{-3}	1.22×10^{-2}
¹⁶⁷ Ir ^m	1.14×10^{-6}	-3.02×10^{-7}	1.26×10^{-5}	1.15×10^{-3}	3.01×10^{-3}	9.13×10^{-3}
¹⁷⁰ Au	1.10×10^{-6}	1.74×10^{-6}	5.47×10^{-6}	6.91×10^{-4}	2.01×10^{-3}	5.92×10^{-3}
¹⁷⁰ Au ^m	-1.13×10^{-6}	2.70×10^{-6}	3.96×10^{-6}	5.03×10^{-4}	1.40×10^{-3}	4.21×10^{-3}
¹⁷¹ Au ^m	5.08×10^{-7}	-6.33×10^{-7}	3.59×10^{-6}	6.15×10^{-4}	1.48×10^{-3}	4.51×10^{-3}
¹⁷¹ Au	1.85×10^{-6}	1.19×10^{-6}	6.49×10^{-6}	6.90×10^{-4}	1.92×10^{-3}	6.01×10^{-3}
¹⁷⁶ Tl	1.94×10^{-6}	1.18×10^{-7}	1.24×10^{-5}	9.58×10^{-4}	2.85×10^{-3}	8.97×10^{-3}
¹⁷⁷ Tl ^m	9.65×10^{-7}	2.39×10^{-8}	1.10×10^{-6}	3.77×10^{-4}	1.14×10^{-3}	3.40×10^{-3}
¹⁷⁷ Tl	-2.24×10^{-6}	1.75×10^{-6}	1.76×10^{-5}	1.28×10^{-3}	3.52×10^{-3}	1.08×10^{-2}
¹⁸⁵ Bi ^m	-2.96×10^{-6}	-3.61×10^{-6}	2.99×10^{-6}	6.32×10^{-4}	1.72×10^{-3}	5.33×10^{-3}

is one key input for calculating nuclear properties [66–68]. In the present work, we plot the relationship between the maximum instantaneous rate of change of the penetration probability and the decay energy for different nuclei in the case of $I_0 = 10^{23}$ W/cm² in Fig. 6. Interestingly, the decay energy Q_p is negatively related to the rate of change of the penetration probability. The smaller the decay energy is, the more sensitive the laser with the same intensity becomes. Using parent nuclei with low proton radioactive decay energy can get a more obvious half-life change rate in future experiments.

B. The chirp to the laser pulse

Since the laser electric field oscillates back and forth with the change of phase, the influence of $\chi_\phi^{(1)}$ in Eq. (38) on the proton radioactivity penetration probability will be mostly canceled out. This results in that even if the maximum instantaneous penetration probability change rate is significant, the average penetration probability change rate within a laser pulse is insignificant. Rizea *et al.* proposed that using short laser pulses of rectangular shape with an odd number of half-cycles yield can increase the decay rate of proton radioactivity by three orders of magnitude [11]. The solution to eliminating

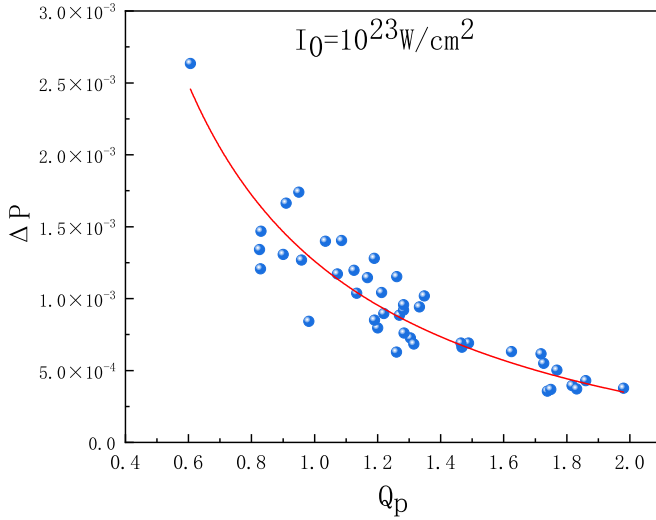


FIG. 6. The relationship between the maximum instantaneous rate of change of the penetration probability and the decay energy for different nuclei in the case of $I_0 = 10^{23}$ W/cm².

half of the electric field is not optimistic with the current technical means. Qi *et al.* proposes an experimental scheme based on elliptically polarized laser fields [33]. Moreover, only the effect of the angle θ between vector $\vec{E}(t)$ and vector \vec{r} are considered on the average rate of change of penetration probability in Ref. [33] (the frequency change was not considered). To obtain a more significant average rate of change in penetration probability, we propose to break the symmetry of the laser electric field by introducing the chirp to the laser pulse. Detuning the laser pulse compressor can generate the asymmetric laser pulses in chirped-pulse amplification laser systems. The sequence of Gaussian chirped-pulse with an envelope function can be written as [69]

$$E(p, b) = E_0 \exp\left(-\frac{p^2}{4\pi^2 x^2}\right) \sin(p + b \times p^2/2\pi), \quad (42)$$

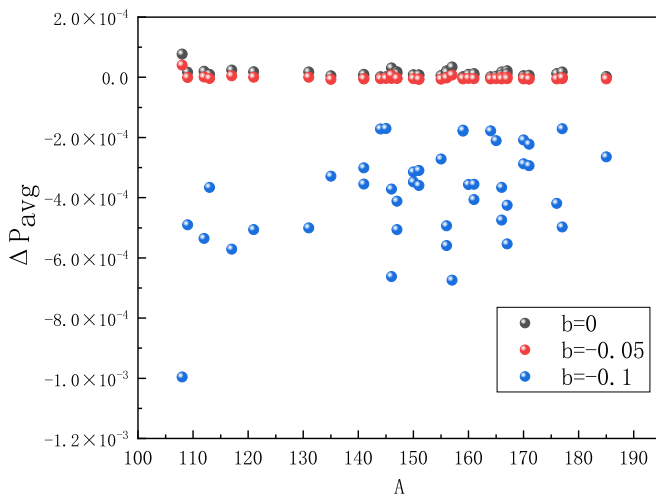


FIG. 7. The influence of a peak intensity of $I_0 = 10^{25}$ W/cm² high-intensity laser on the average rate of change of penetration probability with $b = 0, -0.05, -0.1$.

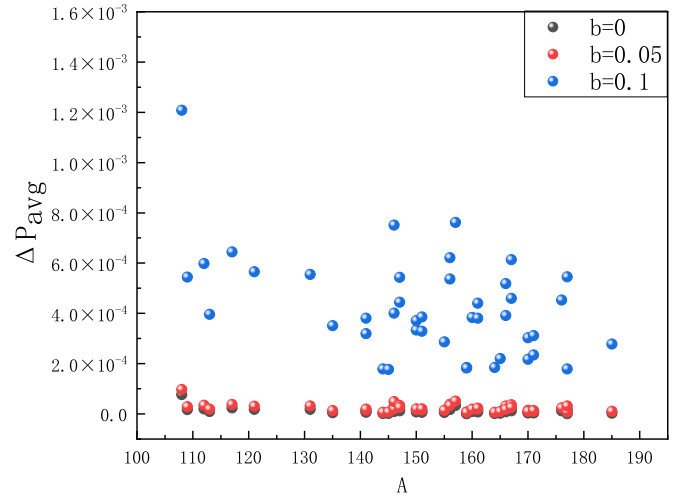


FIG. 8. The influence of a peak intensity of $I_0 = 10^{25}$ W/cm² high-intensity laser on the average rate of change of penetration probability with $b = 0, 0.05, 0.1$.

where b is the chirp parameter. Here, $b < 0$ means a negative chirp and $b > 0$ means a positive chirp.

In the present work, we studied the effect of a high-intensity laser pulse with a peak intensity of $I_0 = 10^{25}$ W/cm² that ELI-NP can deliver in the future on the average rate of change of penetration probability ΔP_{avg} with different chirp values. The detailed results are shown in Figs. 7 and 8, where the x axis represents the mass number, and the y axis represents ΔP_{avg} . The same τ and θ are used as in Fig. 2. As can be seen from Figs. 7 and 8, compared with phase symmetric laser pulses, asymmetric chirp-laser pulses can make ΔP_{avg} more significant. Moreover, the positive chirp-laser pulses increase the penetration probability, while the negative chirp-laser pulses decrease the penetration probability. Therefore, ΔP_{avg} can be enhanced using asymmetric laser pulses with a positive chirp. To make a more intuitive comparison of symmetric

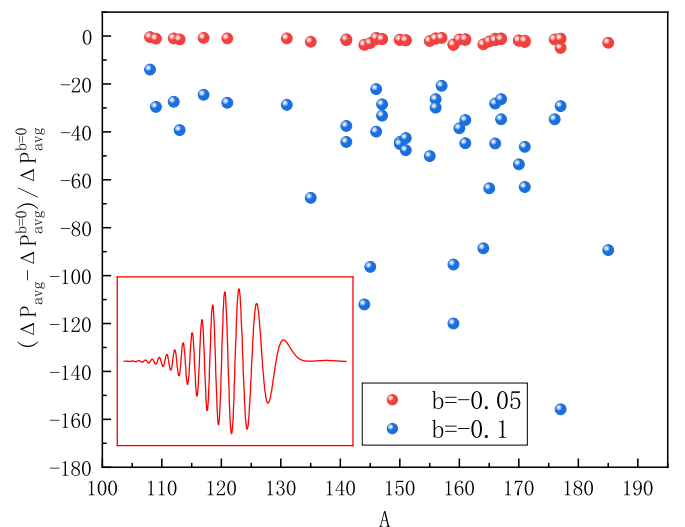


FIG. 9. The growth rate δ of ΔP_{avg} in the cases of $b = -0.05$ and -0.1 .

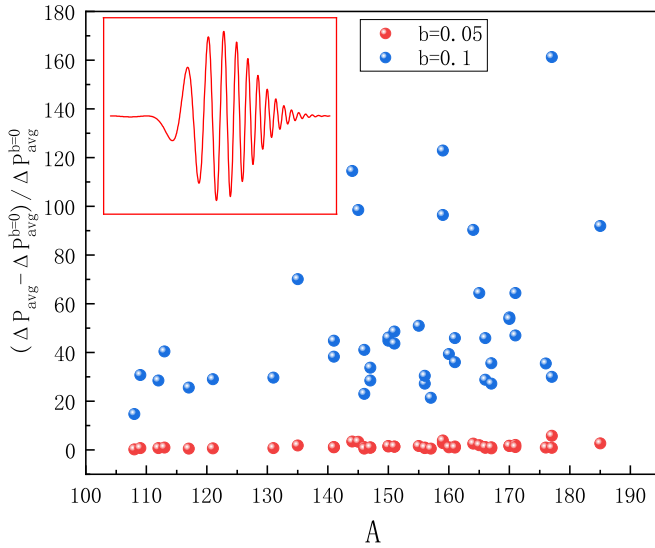


FIG. 10. The growth rate δ of ΔP_{avg} in the cases of $b = 0.05$ and 0.1 .

laser pulses and chirp-laser pulses, the growth rate δ of ΔP_{avg} corresponding to different chirp parameters is shown in Figs. 9 and 10, where $\delta = (\Delta P_{\text{avg}} - \Delta P_{\text{avg}}^{b=0}) / \Delta P_{\text{avg}}^{b=0}$. The schematic diagrams of the laser electric field waveforms corresponding to the negative chirp and the positive chirp are in the red box in the lower left corner and the red box in the upper left corner of Figs. 9 and 10, respectively. From these figures, we can see that the δ increase as the b value increases. Compared with symmetric laser pulses, the maximum δ can reach 160 in the case of $b = 0.1$, which is equivalent to increasing the laser intensity by two orders of magnitude. This result proves that it is feasible to introduce the chirp to the laser pulse to

improve ΔP_{avg} . Moreover, the chirped laser pulse can be adjusted to speed up or delay the half-life of proton radioactivity as needed in future applications.

IV. SUMMARY

In summary, we present a systematic study of the laser-assisted proton radioactivity of deformed nuclei. We use a peak intensity of 10^{23} W/cm² Gaussian laser and aim at obtaining achievable quantitative evaluations of the laser influences on proton radioactivity. The calculation shows that the Gaussian laser affects the proton radioactivity half-life by affecting the penetration probability to some small but finite extent. In particular, it is found that the ^{108}I is the most sensitive parent nuclei to the strong laser pulse. And the decay energy is negatively related to the rate of change of the penetration probability. We propose to use the chirp-laser pulse to obtain a more significant average rate of change in penetration probability. Reasonable use of positive chirp is equivalent to increasing the laser intensity by two orders of magnitude. This can serve as a reference for future theoretical and experimental research on proton radioactivity.

ACKNOWLEDGMENTS

This work was supported by the National Key R&D Program of China (Grant No. 2018YFA0404802), National Natural Science Foundation of China (Grant Nos. 12135009, 11875319), the Science and Technology Innovation Program of Hunan Province (Grant No. 2020RC4020), Research Project of NUDT (Grant No. ZK18-02-02), Fok Ying-Tong Education Foundation (Grant No. 161007), and the Hunan Provincial Innovation Foundation for Postgraduate (Grant No. CX20210007).

- [1] R. Betti and O. Hurricane, *Nat. Phys.* **12**, 435 (2016).
- [2] M. J. C. van Gemert and A. J. Welch, *Laser Surg. Med.* **9**, 405 (1989).
- [3] N. Zamfir, *Eur. Phys. J.: Spec. Top.* **223**, 1221 (2014).
- [4] B. S. Xie, Z. L. Li, and S. Tang, *Matter Radiat. Extremes* **2**, 225 (2017).
- [5] S. N. Chen, F. Negoita, K. Spohr, E. d'Humières, I. Pomerantz, and J. Fuchs, *Matter Radiat. Extremes* **4**, 054402 (2019).
- [6] S. Weng, Z. Sheng, M. Murakami, M. Chen, M. Liu, H. Wang, T. Yuan, and J. Zhang, *Matter Radiat. Extremes* **3**, 28 (2018).
- [7] D. Strickland and G. Mourou, *Opt. Commun.* **56**, 219 (1985).
- [8] G. A. Mourou, T. Tajima, and S. V. Bulanov, *Rev. Mod. Phys.* **78**, 309 (2006).
- [9] J. W. Yoon, C. Jeon, J. Shin, S. K. Lee, H. W. Lee, I. W. Choi, H. T. Kim, J. H. Sung, and C. H. Nam, *Opt. Express* **27**, 20412 (2019).
- [10] J. W. Yoon, Y. G. Kim, I. W. Choi, J. H. Sung, H. W. Lee, S. K. Lee, and C. H. Nam, *Optica* **8**, 630 (2021).
- [11] Ş. Mişicu and M. Rizea, *J. Phys. G* **46**, 115106 (2019).
- [12] K. A. Tanaka, K. M. Spohr, D. L. Balabanski, S. Balascuta, L. Capponi, M. O. Cernaianu, M. Cuciuc, A. Cucoanes, I. Dancus, A. Dhal, B. Diaconescu, D. Doria, P. Ghenuche, D. G. Ghita, S. Kisiov, V. Nastasa, J. F. Ong, F. Rotaru, D. Sangwan, P.-A. Söderström *et al.*, *Matter Radiat. Extremes* **5**, 024402 (2020).
- [13] J.-G. Deng, H.-F. Zhang, and G. Royer, *Phys. Rev. C* **101**, 034307 (2020).
- [14] J.-G. Deng and H.-F. Zhang, *Phys. Rev. C* **102**, 044314 (2020).
- [15] J.-G. Deng and H.-F. Zhang, *Chin. Phys. C* **45**, 024104 (2021).
- [16] J.-H. Cheng, X. Pan, Y.-T. Zou, X.-H. Li, Z. Zhang, and P.-C. Chu, *Eur. Phys. J. A* **56**, 1 (2020).
- [17] Z. Y. Zhang, H. B. Yang, M. H. Huang, Z. G. Gan, C. X. Yuan, C. Qi, A. N. Andreyev, M. L. Liu, L. Ma, M. M. Zhang, Y. L. Tian, Y. S. Wang, J. G. Wang, C. L. Yang, G. S. Li, Y. H. Qiang, W. Q. Yang, R. F. Chen, H. B. Zhang, Z. W. Lu *et al.*, *Phys. Rev. Lett.* **126**, 152502 (2021).
- [18] B. Wang, Z. Ren, and D. Bai, *Phys. Lett. B* **793**, 110 (2019).
- [19] D. Bai, Z. Ren, and G. Röpke, *Phys. Rev. C* **99**, 034305 (2019).
- [20] G. Gamow, *Z. Phys.* **51**, 204 (1928).
- [21] R. W. Gurney and E. U. Condon, *Nature (London)* **122**, 439 (1928).
- [22] Y. Ren and Z. Ren, *Phys. Rev. C* **85**, 044608 (2012).
- [23] Y. T. Oganessian and V. K. Utyonkov, *Rep. Prog. Phys.* **78**, 036301 (2015).

- [24] S. Hofmann, S. Heinz, R. Mann, J. Maurer, G. Münzenberg, S. Antalic, W. Barth, H. Burkhard, L. Dahl, K. Eberhardt *et al.*, *Eur. Phys. J. A* **52**, 1 (2016).
- [25] M. Karny, K. Rykaczewski, R. Grzywacz, J. Batchelder, C. Bingham, C. Goodin, C. Gross, J. Hamilton, A. Korgul, W. Królas, S. Liddick, K. Li, K. Maier, C. Mazzocchi, A. Piechaczek, K. Rykaczewski, D. Schapira, D. Simpson, M. Tantawy, J. Winger *et al.*, *Phys. Lett. B* **664**, 52 (2008).
- [26] D. Ni and Z. Ren, *Phys. Rev. C* **81**, 064318 (2010).
- [27] C. Xu and Z. Ren, *Phys. Rev. C* **69**, 024614 (2004).
- [28] H. M. Castañeda Cortés, C. Müller, C. H. Keitel, and A. Pálffy, *Phys. Lett. B* **723**, 401 (2013).
- [29] Ş. Mişicu and M. Rizea, *J. Phys. G* **40**, 095101 (2013).
- [30] D. S. Delion and S. A. Ghinescu, *Phys. Rev. Lett.* **119**, 202501 (2017).
- [31] D. P. Kis and R. Szilvasi, *J. Phys. G* **45**, 045103 (2018).
- [32] D. Bai, D. Deng, and Z. Ren, *Nucl. Phys. A* **976**, 23 (2018).
- [33] J. Qi, T. Li, R. Xu, L. Fu, and X. Wang, *Phys. Rev. C* **99**, 044610 (2019).
- [34] A. Pálffy and S. V. Popruzhenko, *Phys. Rev. Lett.* **124**, 212505 (2020).
- [35] C. Xu and Z. Ren, *Phys. Rev. C* **73**, 041301(R) (2006).
- [36] M. Ismail, W. Seif, A. Adel, and A. Abdurrahman, *Nucl. Phys. A* **958**, 202 (2017).
- [37] Z. Ren and C. Xu, *Mod. Phys. Lett. A* **23**, 2597 (2008).
- [38] M. Hosseini-Tabatabaei, S. Alavi, and V. Dehghani, *Can. J. Phys.* **99**, 24 (2021).
- [39] D. Ni and Z. Ren, *Phys. Rev. C* **83**, 067302 (2011).
- [40] A. Coban, O. Bayrak, A. Soylu, and I. Boztosun, *Phys. Rev. C* **85**, 044324 (2012).
- [41] A. Soylu and S. Evlice, *Nucl. Phys. A* **936**, 59 (2015).
- [42] C. Xu and Z. Ren, *Phys. Rev. C* **78**, 057302 (2008).
- [43] B. Buck, A. C. Merchant, and S. M. Perez, *Phys. Rev. C* **45**, 2247 (1992).
- [44] S. Cwiok, J. Dudek, W. Nazarewicz, J. Skalski, and T. Werner, *Comput. Phys. Commun.* **46**, 379 (1987).
- [45] J.-L. Chen, X.-H. Li, J.-H. Cheng, J.-G. Deng, and X.-J. Wu, *J. Phys. G* **46**, 065107 (2019).
- [46] K. P. Santhosh and I. Sukumaran, *Phys. Rev. C* **96**, 034619 (2017).
- [47] V. Y. Denisov and H. Ikezoe, *Phys. Rev. C* **72**, 064613 (2005).
- [48] K. N. Huang, M. Aoyagi, M. H. Chen, B. Crasemann, and H. Mark, *At. Data Nucl. Data* **18**, 243 (1976).
- [49] J. J. Morehead, *J. Math. Phys.* **36**, 5431 (1995).
- [50] N. Takigawa, T. Rumin, and N. Ihara, *Phys. Rev. C* **61**, 044607 (2000).
- [51] M. Ismail, W. Seif, and H. El-Gebaly, *Phys. Lett. B* **563**, 53 (2003).
- [52] Z. Gao-Long, L. Xiao-Yun, and L. Zu-Hua, *Chin. Phys. Lett.* **25**, 1247 (2008).
- [53] P. Möller, A. Sierk, T. Ichikawa, and H. Sagawa, *At. Data Nucl. Data Tables* **109–110**, 1 (2016).
- [54] D. Delion, R. Liotta, and R. Wyss, *Phys. Rep.* **424**, 113 (2006).
- [55] W. Huang, M. Wang, F. Kondev, G. Audi, and S. Naimi, *Chin. Phys. C* **45**, 030002 (2021).
- [56] M. Wang, W. Huang, F. Kondev, G. Audi, and S. Naimi, *Chin. Phys. C* **45**, 030003 (2021).
- [57] F. Kondev, M. Wang, W. Huang, S. Naimi, and G. Audi, *Chin. Phys. C* **45**, 030001 (2021).
- [58] B. Blank and M. Borge, *Prog. Part. Nucl. Phys.* **60**, 403 (2008).
- [59] T. Brabec, M. Y. Ivanov, and P. B. Corkum, *Phys. Rev. A* **54**, R2551 (1996).
- [60] J. Chen, J. Liu, L. B. Fu, and W. M. Zheng, *Phys. Rev. A* **63**, 011404(R) (2000).
- [61] J. Dong, W. Zuo, J. Gu, Y. Wang, and B. Peng, *Phys. Rev. C* **81**, 064309 (2010).
- [62] H. F. Zhang, Y. J. Wang, J. M. Dong, J. Q. Li, and W. Scheid, *J. Phys. G: Nucl. Part. Phys.* **37**, 085107 (2010).
- [63] J. M. Dong, H. F. Zhang, and G. Royer, *Phys. Rev. C* **79**, 054330 (2009).
- [64] Y. Qian and Z. Ren, *Eur. Phys. J. A* **52**, 68 (2016).
- [65] D. S. Delion and A. Dumitrescu, *Phys. Rev. C* **103**, 054325 (2021).
- [66] J.-G. Deng and H.-F. Zhang, *Phys. Lett. B* **816**, 136247 (2021).
- [67] J.-G. Deng, J.-C. Zhao, J.-L. Chen, X.-J. Wu, and X.-H. Li, *Chin. Phys. C* **42**, 044102 (2018).
- [68] J.-G. Deng, J.-H. Cheng, B. Zheng, and X.-H. Li, *Chin. Phys. C* **41**, 124109 (2017).
- [69] X. Zhang, B. Shen, L. Ji, W. Wang, J. Xu, Y. Yu, L. Yi, X. Wang, N. A. Hafz, and V. Kulagin, *Phys. Plasmas* **19**, 053103 (2012).